Journal of Catalysis 460 (2026) 116954

Contents lists available at ScienceDirect

Journal of Catalysis

journal homepage: www.elsevier.com/locate/jcat

Hemilability-controlled reactivity and hydride-mediated activation in Mn(I)-catalysed dehydrogenative Si–O bond formation

Susana García-Abellán [a], Jorge Gonzalo [b], Andrea Pérez-García [b], Miguel A. Casado [b], Pilar García-Orduña [a], Vincenzo Passarelli [a], Julen Munárriz [b,**], Manuel Iglesias [b,*]

[a] Instituto de Síntesis Química y Catálisis Homogénea (ISQCH), CSIC-Universidad de Zaragoza, C/Pedro Cerbuna 12, 50009 Zaragoza, Spain
[b] Instituto de Biocomputación y Física de Sistemas Complejos (BIFI), Departamento de Química Física, Universidad de Zaragoza 50009 Zaragoza, Spain

ARTICLE INFO

Keywords:
Catalysis
Hydrogen
Manganese
Silanes

ABSTRACT

Manganese(I) complexes supported by hemilabile P-N ligands based on a 1,2,3-triazole scaffold have been synthesized and evaluated as catalysts for the dehydrogenative coupling of hydrosilanes with hydroxyl compounds. Structural and spectroscopic studies, including single-crystal X-ray diffraction, confirmed the bidentate coordination of these ligands in complexes **1**–**5**. Catalytic tests demonstrated that the ligand identity has a pronounced effect on the activity, with more labile triazole moieties showing superior performance. Notably, the use of $LiHBEt_3$ (1:1 M ratio with **1**) enabled in situ generation of a manganese hydride species, significantly enhancing the reactivity in the methanolysis of hydrosilanes, where turnover frequencies above 45,000 h^{-1} were achieved. DFT calculations suggest that the reaction proceeds via a concerted pathway requiring triazole moiety dissociation, providing a mechanistic basis for the role of ligand hemilability in the activation of the hydrosilane.

1. Introduction

Manganese complexes are inexpensive, readily available, and generally exhibit low toxicity compared to precious-metal catalysts, making them attractive alternatives for sustainable catalytic processes. Among these, Mn(I) carbonyl complexes have garnered particular attention due to their versatile reactivity and catalytic activity in key transformations such as carbon dioxide reduction [1,2], as well as hydrogenation and dehydrogenation reactions [3].

Recent studies have highlighted the potential of Mn(I) complexes in silicon–oxygen bond formation by the dehydrogenative coupling of hydrosilanes with alcohols or water.[4] These reactions play a central role in organosilicon chemistry, allowing for the synthesis of silanols, siloxanes, and alkoxysilanes [5,6]. Noteworthy examples include the $[Mn_2(CO)_{10}]$/TPPO (TPPO = triphenylphosphine oxide) system reported by Meng and co-workers for the silylation of alcohols [7], and the $MnBr(CO)_5$ hydrolysis catalyst disclosed by Leitner, Werlé and coworkers [8]. In the case of the former, a binuclear active species has been proposed. The TPPO ligand coordinates to one of the Mn centres, which undergoes oxidative addition of the Si–H bond. Subsequently, reaction with the corresponding alcohol generates molecular hydrogen and a methoxide complex. Upon reductive elimination, this complex produces the silyl ether and regenerates the active species. Notably, all intermediates in the catalytic cycle are binuclear. Other examples that employ binuclear manganese catalysts have been reported for the alcoholysis of silanes [9,10]. In the absence of TPPO ligand, Mn–Mn bond cleavage of $[Mn_2(CO)_{10}]$ by binuclear oxidative addition of the Si–H bond has been described [9]. In the case of the $[MnBr(CO)_5]$ catalyst, a Luo-Crabtree-type mechanism, which involves the heterolytic cleavage of the silane, has been proposed. The active species, $[MnH(CO)_3(L)_2]$, is suggested to form by oxidative addition of the hydrosilane, followed by the reductive elimination of the resulting silyl bromide adduct.

The use of $[MnBr(CO)_5]$ as catalyst has also been reported to enable the dehydrogenative coupling of primary, secondary and tertiary alcohols with the monohydrosilane ethyl (2*S*)-2-[(diisopropylsilyl)oxy] propanoate, thus allowing for the preparation of a variety of unsymmetrical bisalkoxysilanes [11]. The related complex [mer-$Mn(CO)_3${P

* Corresponding author at: Instituto de Síntesis Química y Catálisis Homogénea (ISQCH), CSIC-Universidad de Zaragoza, C/Pedro Cerbuna 12, 50009-Zaragoza, Spain.
** Corresponding author at: Instituto de Biocomputación y Física de Sistemas Complejos (BIFI), Departamento de Química Física, Universidad de Zaragoza, 50009 Zaragoza, Spain.
E-mail addresses: julen@unizar.es (J. Munárriz), miglesia@unizar.es (M. Iglesias).

https://doi.org/10.1016/j.jcat.2026.116954
Received 28 January 2026; Received in revised form 5 May 2026; Accepted 6 May 2026
Available online 14 May 2026

$(OCH_2)_3CMe\}_2(CH_2Cl_2)]BAr^F$ has been reported to catalyse the coupling of phenol and hydrosilanes via a mechanism that entails the formation of a silane σ complex, followed by heterolytic cleavage of the Si–H bond [12].

Mn(V) precatalysts based on the [MnN(salen-3,5-^{t}Bu$_2$)] framework have been reported to exhibit high efficiency in catalysing the alcoholysis and hydrolysis of hydrosilanes [13–16]. It has been proposed that, under the reaction conditions, the Mn(V) precatalyst undergoes in situ reduction to generate Mn(II) or Mn(III) species, which constitute the catalytically active forms.

These advances underscore the emerging potential of Mn-based catalysts as sustainable substitutes for noble metals in Si–O bond formation, yet homogeneous systems utilizing Earth-abundant metals are still limited. Moreover, the concurrent generation of hydrogen in these reactions, combined with the low toxicity and stability of organosilanes, has stimulated interest in their application as hydrogen storage systems [17]. Despite this, studies on Mn catalysts have predominantly focused on organosilane synthesis, often overlooking hydrogen evolution from polyhydrosilanes (vide supra). A deeper understanding of the structure–activity relationships and mechanistic aspects governing Mn-catalysed dehydrogenative methanolysis and hydrolysis is still lacking, warranting further investigation.

Hemilabile ligands provide easily accessible coordination sites while ensuring robust catalysts. In this regard, 1,2,3-triazole ligands have been categorized into three types based on their coordination behaviour: A-, B-, and C-type (Fig. 1). A-type ligands, the so-called "normal" coordination mode [18], possess a donor group at the C4 position, and coordinate to a metal centre through both N3 and the donor group, forming a stable chelating structure [18–28]. Less common B-type ligands, described as "inverse" coordination, are functionalized at N1 and typically coordinate through N2 owing to the chelate effect [19,27–34], though in some cases, N3 coordination prevails due to its higher stability [27,31]. C-type ligands, characterized by N2 substitution, remain unexplored, except for a recent example reported by us [35]. **A**-type ligands have been shown to form more stable chelates due to the greater electron density and stronger π back-donation by the N3. Consequently, B- and C-type 1,2,3-triazoles are more likely to enable a hemilabile behaviour.

The iridium complexes of general formula [IrCl(COD)**L**], previously reported by our group, bearing ligands **L1**, **L2** [35], and **L3** [32] (Fig. 2), exhibit catalytic activities for formic acid dehydrogenation that are highly sensitive to the nature of the triazole donor group. In this system, the formation of more stable chelate structures markedly enhances catalytic performance by stabilizing key intermediates within the catalytic cycle [35].

At this point, it should be noted that the reported catalytic applications of Mn(I)-PN systems remain scarce. Key examples include the hydrogenation of carboxylic acid esters [36,37], ketones [38–41], and carbon double bonds [42]. Additionally, these systems have been successfully applied to the dimerization of terminal alkynes and the hydroboration of styrene derivatives [43], as well as in Guerbet reactions for the upgrading of ethanol to butanol derivatives.[44,45].

Building on our recent studies of P-N hemilabile ligands [32,35], and the development of Earth-abundant metal catalysts for Si–O bond formation via dehydrocoupling reactions [46], we now report the synthesis

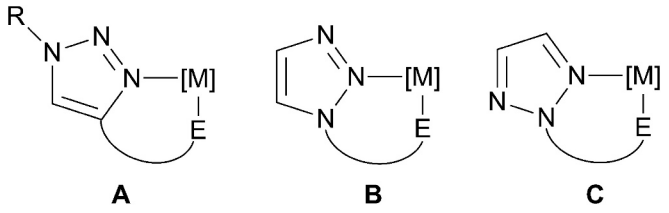

Fig. 1. Depiction of A-, B-, and C-type bidentate 1,2,3-triazole ligands.

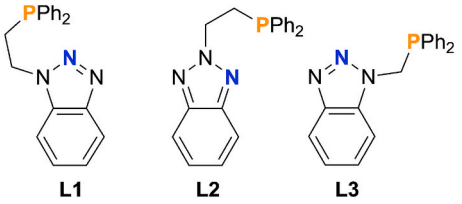

Fig. 2. Depiction of **L1**, **L2** and **L3**.

of a new family of Mn(I) catalysts supported by ligands **L1**-**L3**. Evaluation of their catalytic performance in the dehydrogenative coupling of hydrosilanes with hydroxyl compounds, as determined from H_2 evolution, uncovered a pronounced dependence on the ligand structure. This correlation provides a rational basis for catalyst optimization through controlled modulation of ligand hemilability.

To gain deeper insight into the observed reactivity, a combination of experimental and computational investigations was undertaken. These studies shed light on the reaction mechanism, highlighting the crucial role of the ligand's hemilabile nature and the formation of a Mn–hydride active species, whose in situ generation markedly enhances the catalytic performance.

2. Results and discussion

2.1. Synthesis and characterization of Mn(I) complexes

The synthesis of neutral complexes of the type [MnBr(CO)$_3$(P-N)] was carried out by reacting [MnBr(CO)$_5$] with the corresponding ligand in a 1:1 stoichiometry (Scheme 1) at 80 °C in acetonitrile. Both the reaction of **L1** and **L2** with [MnBr(CO)$_5$] resulted in the formation of sparingly soluble complexes that were not characterized in solution. Addition of $AgBF_4$ renders cationic complexes **1** and **2**, which are soluble in CD_3CN. In sharp contrast with **L1** and **L2**, the reaction of **L3** with [MnBr(CO)$_5$] at 80 °C does result in the formation of a neutral complex that is soluble in acetonitrile (**3**) which was isolated and characterized. Furthermore, addition of $AgBF_4$ to a solution of **3** in CH_3CN allowed for the synthesis of the cationic complex **4**.

The bidentate coordination of the P-N ligands was confirmed by NMR spectroscopy in all cases, as evidenced by the diastereotopic nature of the signals corresponding to the methylenic protons in the ^{1}H NMR spectra (Fig. 3). This also confirms the exclusive formation of the *fac*-(CO)$_3$ isomer in all cases.

For **1**, these signals overlap, showing only two multiplets, each

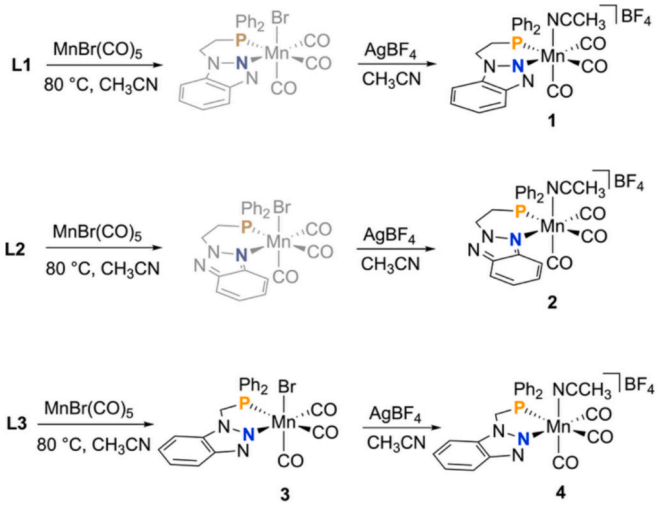

Scheme 1. Synthesis of complexes **1**, **2**, **3**, and **4**. Complexes in grey were not isolated.

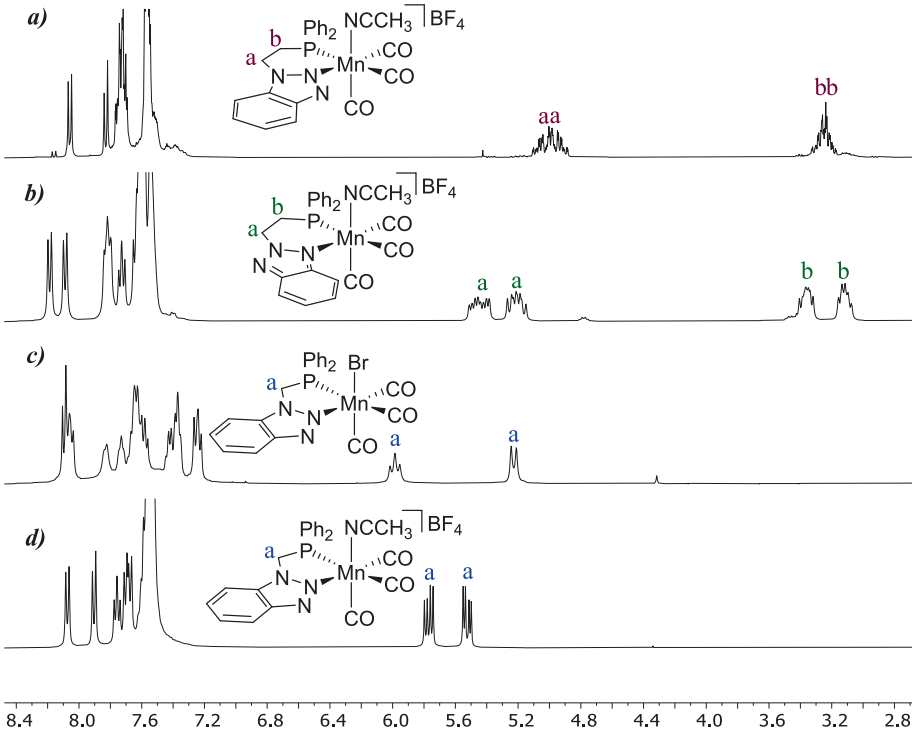

Fig. 3. ^{1}H NMR spectra of: *a*) **1**; *b*) **2**; *c*) **3** and *(d)* **4**; in CD_3CN.

integrating for 2H, at δ 5.09–4.83 and 3.31–3.14 ppm for NCH_2 and CH_2P, respectively (Fig. 3a). For **2**, they appear as four multiplets, two

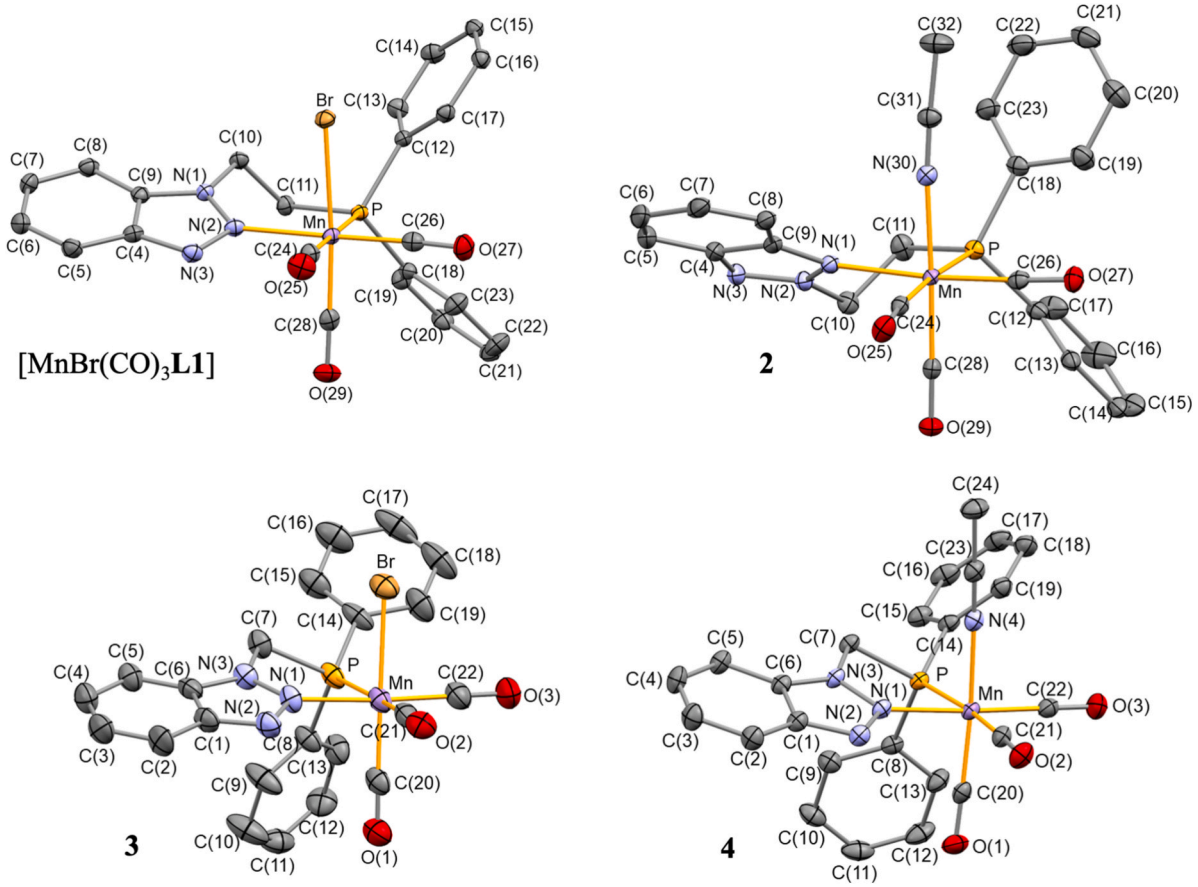

Fig. 4. Molecular structure of [MnBr(CO)$_3$**L1**], **2**, **3** in **3**·0.5($C_4H_{10}O$), and **4** in **4**·CH_3CN, with ellipsoids at 50 % probability. Hydrogen atoms have been omitted for clarity.

corresponding to the NCH_2 protons at δ 5.52–5.37 and 5.28–5.13 ppm, and two corresponding to the CH_2P protons at δ 3.42–3.31 and 3.18–3.05 ppm, each integrating 1H (Fig. 3b). For the pair of complexes synthesized from **L3** (**3** and **4**), a signal is observed for each methylene proton. The first one shows an apparent triplet and a broad doublet at δ 5.99 and 5.23 ppm, with coupling constants of 12.6 and 13.2 Hz, respectively (Fig. 3c). In contrast, the second one shows two doublets of doublets at δ 5.77 and 5.52 ppm, with coupling constants of 15.0 and 7.2 Hz for the first one, and 15.0 and 5.8 Hz for the second one (Fig. 3d).

The $^{31}P\{^1H\}$ NMR spectrum also confirms the coordination of the phosphane moiety of the ligands to the metal centre, with the phosphorus nucleus resonances at δ 41.5, 43.5, 65.2, and 71.6 ppm for **1**, **2**, **3**, and **4**, respectively.

In the $^{13}C\{^1H\}$ APT NMR spectrum, the carbon nuclei of the carbonyl ligands are not observed, as seen in some analogous examples described in the literature. Despite this, the presence of the three carbonyl ligands can be confirmed by FTIR, appearing as intense bands at 2045, 1974 and 1939 cm^{-1} for **1**; at 2043, 1935 and 1883 cm^{-1} for **2**; at 2028, 1952 and 1920 cm^{-1} for **3**; and at 2049, 1971 and 1949 cm^{-1} for **4**. Additionally, for the cationic complexes, **1**, **2**, and **4**, an intense band corresponding to the BF_4^- counterion is also observed at 1052, 1051, and 1019 cm^{-1}, respectively.

Cooling a saturated solution of [MnBr(CO)$_3$**L1**] in acetonitrile and slow diffusion of diethyl ether into concentrated solutions of **2**, **3**, and **4** in acetonitrile allowed for the crystallization of suitable crystals for single-crystal X-ray diffraction analysis (Fig. 4). For all of them, the proposed connectivity was confirmed, obtaining structures with slightly distorted octahedral geometries.

The bite angle for [MnBr(CO)$_3$**L1**] is 92.07(5)°, while for the cationic complex **2** synthesized from **L2** is 90.68(5)°. For complexes containing **L3** and thus leading to the formation of five-membered chelate rings, this angle takes the value of 80.97(11) and 80.60(3)°, for **3** and **4**, respectively. Mn–P bond distances are similar for the complexes [MnBr(CO)$_3$**L1**] and **2**, at 2.3380(5) and 2.3350(5) Å, respectively, as well as the Mn–N distances, 2.0763(16) and 1.9985(16) Å. However, for **3** and **4**, Mn-P distances are slightly shorter: 2.3240(14) and 2.3058(4) Å. The Mn-N distances for **3** and **4** are 2.047(4) and 2.0299(11) Å, respectively.

In all four structures, the substituted N atoms of the benzotriazole exhibit the geometry expected for sp^2 hybridization. However, a slight quaternization is observed for the N atoms of the triazole coordinated to the metal centre, resulting in pitch angles of 6.2, 5.3, and 6.6° for [MnBr(CO)$_3$**L1**], **2**, and **3**, respectively. However, for the coordinated N atom in **4**, a geometry closer to the ideal one expected for sp^2 hybridization is observed, with a pitch angle of 0.3°.

Interestingly, upon dissolving crystals of **2** in CD_3CN, the progressive appearance of a second complex at lower concentration was observed using ^1H NMR spectroscopy. The formation of this second complex can be attributed to the substitution of the triazole by a solvent molecule, due to the large excess of CD_3CN. This postulation is supported by the ^1H NMR spectrum, as the methylene protons in **2** are no longer diastereotopic in the new complex. The ^1H–^{13}C HSQC NMR spectra shows that these methylene protons correlate to two new peaks in the APT NMR (Fig. 5). Additionally, in the $^{31}P\{^1H\}$ NMR spectrum, a new resonance emerges at δ 38.7 ppm.

It is noteworthy that this behaviour is not observed in **1**, **3**, and **4**, which contain type **B** ligands, **L1** and **L3**. The higher lability of the triazole in the complex **2** containing **L2**, of type **C**, is plausibly related to greater steric repulsions between the benzotriazole and the

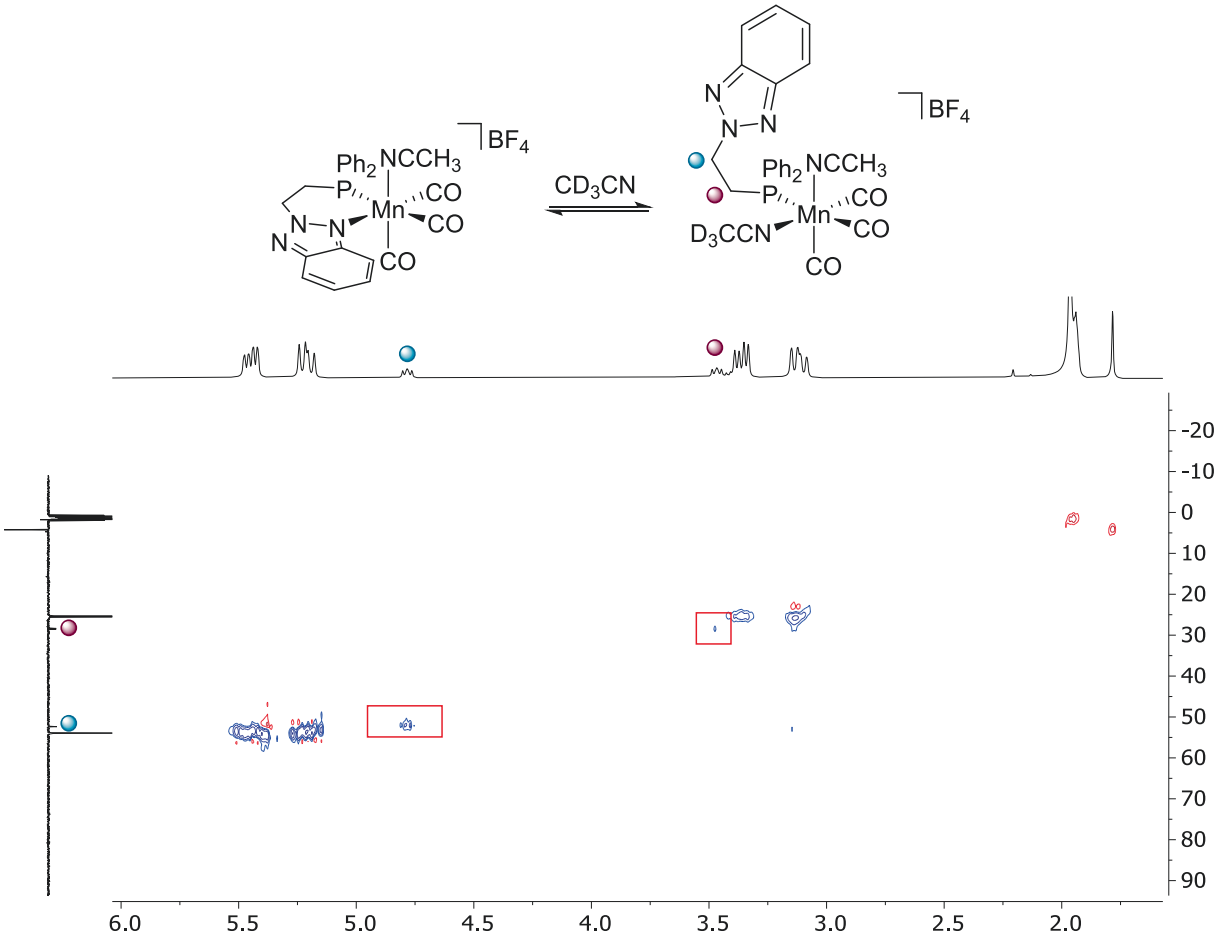

Fig. 5. ^1H–^{13}C HSQC NMR spectrum in CD_3CN of **2** in equilibrium with [Mn(CO)$_3$**L2**$(CD_3CN)_2$][BF_4].

neighbouring carbonyl ligand, which is in line with the behaviour previously reported by us for related Ir and Rh complexes [35].

Subsequently, the reactivity of [$MnBr(CO)_5$] with two equivalents of **L3** was investigated, following a procedure analogous to that employed for the synthesis of **4**, but utilizing a ligand-to-metal-to-$AgBF_4$ ratio of 2:1:1. Under these conditions, complex **5** was selectively obtained (Scheme 2).

The $^{31}P\{^1H\}$ NMR spectrum of **5** shows a single broad signal at δ 84.4 ppm, suggesting the chemical equivalence of the two phosphorus nuclei coordinated to the metal centre. In the ^1H NMR spectrum, the methylene protons appear as two doublets of multiplets centred at δ 5.78 and 5.71 ppm, integrating four protons (Fig. 6a). The geminal methylene protons of each P-N ligand are diastereotopic due to their distinct chemical environments, as supported by the $^1H\{^{31}P\}$ NMR spectrum, which shows two doublets centred at δ 5.78 and 5.71 ppm (Fig. 6b). However, as a consequence of the C_2 symmetry of complex **5**, the methylene protons of one ligand are chemically equivalent to those of the other ligand. In the $^{13}C\{^1H\}$ APT NMR spectrum, the carbon nuclei of the CH_2P groups, both chemically equivalent, appear as a doublet of doublets at δ 49.3 ppm, with phosphorus coupling constants of 12.1 Hz (one-bond coupling) and 10.8 Hz (three-bond coupling), respectively (Fig. 6c). As with the previously studied complexes, no carbon nuclei corresponding to the carbonyl ligands were observed in the $^{13}C\{^1H\}$ APT NMR spectrum of **5**. Nevertheless, the IR spectrum displays bands at 1953 and 1890 cm^{-1}, corresponding to the two possible vibrational modes of the two carbonyl ligands. Additionally, a strong band is observed at 1031 cm^{-1}, corresponding to the BF_4^- counterion.

Single crystals suitable for X-ray diffraction analysis were obtained by slow diffusion of diethyl ether into a concentrated acetonitrile solution of **5** (Fig. 7).

The crystal structure confirmed the bidentate coordination of the two **L3** ligands to the metal centre. As suggested by the equivalence of the phosphorus nuclei observed in the $^{31}P\{^1H\}$ NMR spectrum, the second phosphine ligand is coordinated *trans* to the first. The P(1)–Mn–N(3) and P(2)–Mn–N(5) bite angles are 81.88(4)° and 82.78(4)°, respectively, consistent with those found for **3** and **4** [80.97(11)° and 80.60(3)°, respectively]. The Mn–P(1) and Mn–P(2) bond lengths, 2.2850(5) and 2.2702(5) Å, respectively, are notably shorter than those observed for **3** and **4** [2.3240(14) and 2.3058(4) Å, respectively]. Although this observation might appear inconsistent with the stronger *trans* influence of the phosphine ligand compared to the carbonyl, it can be rationalized by the reduced number of carbonyl ligands (two in **5**), which leads to a decreased metal-to-ligand back-donation. As a result, the higher electron density at the metal centre in **5** relative to **3** and **4** could account for the observed bond shortening. With regard to the P-N ligands, both the substituted and coordinated nitrogen atoms show slight quaternization. The pitch angles for N(3) and N(5) are 6.1° and 3.3°, respectively.

2.2. Catalytic activity of Mn(I) complexes

The limited number of examples of manganese-catalysed dehydrogenative coupling between hydrosilanes and alcohols or water prompted us to investigate how fine-tuning Mn catalysts through hemilability control could enhance their activity.

Initial catalytic tests were conducted to evaluate the relative activity

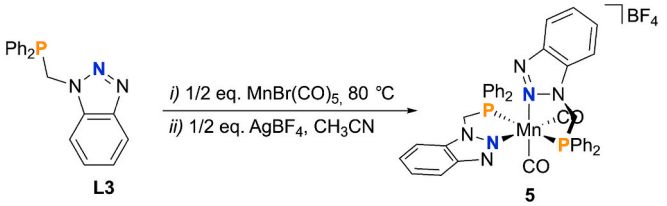

Scheme 2. Synthesis of **5**.

of complexes **1**–**5** in the dehydrogenative coupling of hydrosilanes with water (Fig. 8). The reactions were carried out at 50 °C in a 1:1 H_2O:THF mixture, using $PhSiH_3$ as the substrate and a catalyst loading of 1 mol%. The best catalytic activities were obtained for complexes **1** and **2**, which feature the most labile triazole groups. It is worth mentioning that both catalysts generate H_2 in a 3:1 ratio relative to $PhSiH_3$ upon reaction completion, indicating complete hydrolysis of all three Si–H bonds. The resulting residue is an insoluble solid, which can be attributed to the formation of crosslinked siloxane networks.

Complex **4** is significantly more active than the related complexes **3** and **5**, which feature the same ligand. This enhanced activity is likely due to the greater availability of coordination sites in **4**, as complex **3** bears a Br ligand and complex **5** includes two PN ligands that limit coordination.

Although catalyst **2** exhibits a higher initial TOF than **1** (1380 h^{-1} and 900 h^{-1}, respectively), **1** reaches full conversion in a shorter reaction time, plausibly due to the gradual loss of activity for catalyst **2** over the course of the reaction as a consequence of the lower stability arising from the more labile triazole moiety. Moreover, synthetic challenges render ligand **L2** less accessible. Based on these considerations, complex **1** was selected for further optimization of the reaction conditions.

Various H_2O/silane ratios were investigated to evaluate the effect of excess water on the kinetics of the reaction. The initially studied 1:1 H_2O:THF mixture employed water as a cosolvent (0.25 mL, 13.9 mmol). Reducing the water amount to 4.5 mmol, corresponding to a 9:1 H_2O:$PhSiH_3$ ratio, resulted in a marked decrease of the initial TOF to 360 h^{-1}. A further decrease in the H_2O:$PhSiH_3$ ratio to 4.5:1 led to a TOF of 210 h^{-1}, thereby confirming the observed trend (Fig. S42).

In an attempt to enhance the performance of **1**, $LiHBEt_3$ was employed to generate a Mn–hydride complex in situ, which we hypothesized to be the catalytically active species in accordance with literature precedents.[8] The activity of the in situ generated species was studied under conditions otherwise analogous to those explored above for a 1:1 H_2O:THF mixture, showing a significantly improved performance, with an initial TOF value of 1020 h^{-1} (360 h^{-1} in the absence of $LiHBEt_3$). $LiHBEt_3$ was employed in a 1:1 ratio with respect to the Mn precatalyst (both at 1 mol% relative to the silane).

Attempts to hydrolyse secondary and tertiary silanes under the optimized reaction conditions (1:1 H_2O:THF mixture, 50 °C, 1 mol% of **1** and 1 mol% of $LiHBEt_3$) led to low activities and conversions (Fig. 9).

Subsequently, the methanolysis of $PhSiH_3$ was explored under similar conditions (1:1 MeOH:THF mixture, 50 °C, 1 mol% of **1**) with and without $LiHBEt_3$ (Fig. 10). Compared to the hydrolysis reactions, a sharper activation effect was observed in this case in the presence of 1 mol% $LiHBEt_3$, with the initial TOF increasing from 920 to 45630 h^{-1}, reaching full conversion in less than 1 min. Analogously to the hydrolysis reaction, H_2 was generated in a 3:1 ratio relative to $PhSiH_3$, which suggests the selective formation of $PhSi(OCH_3)_3$. This was confirmed by ^1H NMR of the crude (Fig. S47).

No significant improvement of the catalytic activity was observed upon an increase of the MeOH:THF ratio to 4:1. Subsequently, the possibility of using stoichiometric amounts of MeOH (3 equiv) was assessed. In the absence of $LiHBEt_3$, no catalytic activity was observed; however, the addition of 1 mol% $LiHBEt_3$ allows for a 95 % conversion within 25 min with an initial TOF of 3924 h^{-1}. The use of 9 equivalents of MeOH significantly enhances the catalytic activity, achieving full conversion within 7 min, with an initial TOF of 32622 h^{-1}.

The reactivity of secondary and tertiary silanes was also evaluated (Fig. 11), employing a 4:1 MeOH:THF ratio, at 50 °C, with 1 mol% of **1** and 1 mol% of $LiHBEt_3$.

The use of Ph_2SiH_2 leads to full conversion within 25 min (TOF_i = 7560 h^{-1}); as the generation of a 2:1 M ratio of H_2 relative to Ph_2SiH_2 was observed. This suggests the selective formation of $Ph_2Si(OCH_3)_2$, which was confirmed by ^1H NMR of the crude (Fig. S48).

In the case of Et_2SiH_2, after 25 min, a 37 % conversion is observed, with a TOF_i of 1960 h^{-1}. The monohydrosilanes Me_2PhSiH and Ph_3SiH

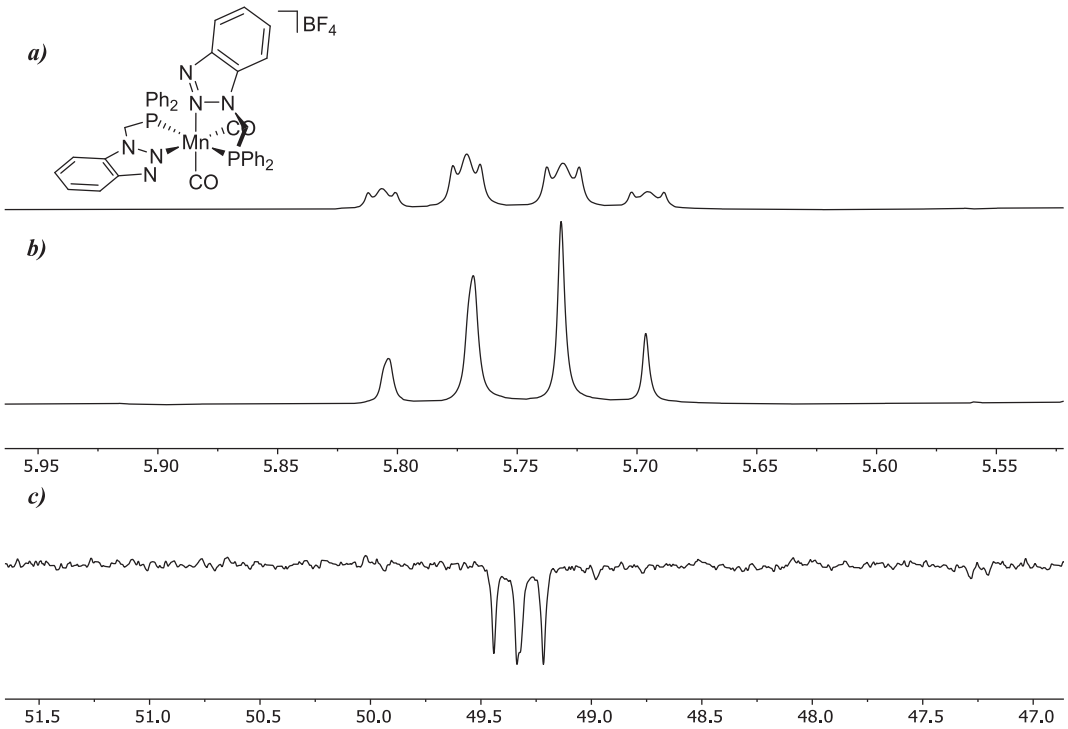

Fig. 6. NMR spectra of **5** in CD_3CN: *a*) ^1H NMR; *b*) $^1H\{^{31}P\}$ NMR; *c*) $^{13}C\{^1H\}$ APT.

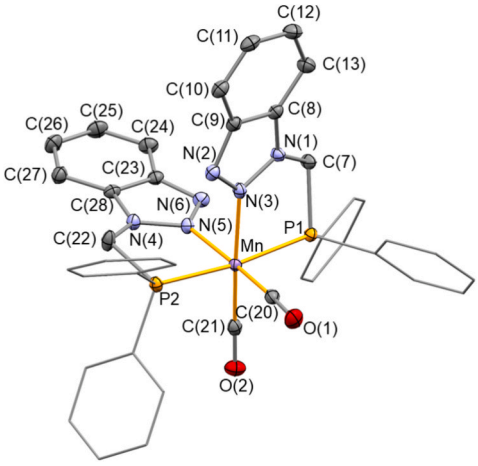

Fig. 7. Molecular structure of **5** in 5·2CH_3CN with thermal ellipsoids drawn at the 50 % probability level. For clarity, the BF_4^- counterion and hydrogen atoms have been omitted, and the phenyl groups of both ligands are shown in a simplified style.

achieve conversions of approximately 12 % after 80 min, whereas $(Me_3SiO)_2MeSiH$ reaches a conversion of over 60 % within the same timeframe.

The performance limits of this catalytic system in the methanolysis of $PhSiH_3$ and Ph_2SiH_2 were investigated through the sequential addition of silane aliquots. In both cases, catalyst activity and stability were assessed over 10 consecutive runs, with no significant loss of activity. Cumulatively, turnover numbers (TONs) of 3000 for $PhSiH_3$ and 2000 for Ph_2SiH_2 were achieved across the 10 cycles (Figs. S43 and S44). In addition, to assess the nature and robustness of the catalytic system, a mercury drop test was performed. No significant decrease in catalytic activity was observed over multiple runs, suggesting that the reaction is unlikely to proceed via nanoparticle-mediated pathways. Furthermore, the fact that the catalyst maintains its activity over successive runs

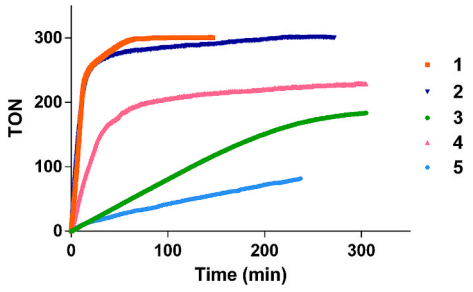

Fig. 8. Conversion over time for the hydrolysis of $PhSiH_3$ with catalysts **1**–**5**. Reaction conditions: 1 mol% of catalyst, 0.5 mmol of $PhSiH_3$, 0.5 mL of a 1:1 mixture H_2O:THF at 50 °C.

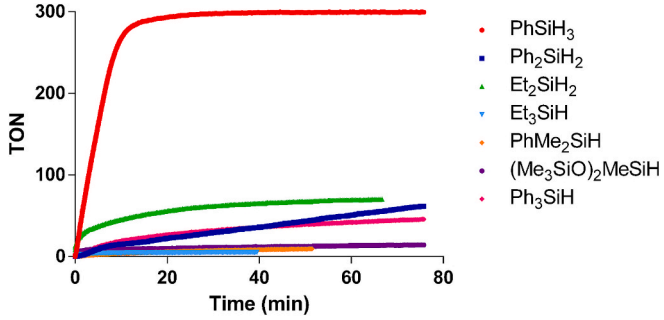

Fig. 9. Conversion over time for the hydrolysis of different silanes with catalyst **1**. Reaction conditions: 1 mol% of **1**, 1 mol% of $LiHBEt_3$, 0.5 mmol of silane, 0.5 mL of a 1:1 mixture H_2O:THF at 50 °C.

further supporting its stability.

To experimentally confirm the proposed in situ generation of the hydride species responsible for the results described above, the reaction of **1** with 1 equiv. of $LiHBEt_3$ was studied in THF-d_8 using a Young NMR

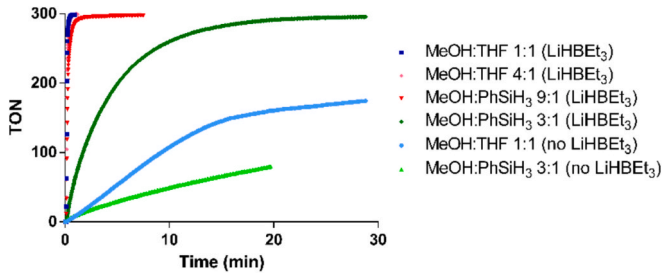

Fig. 10. Conversion over time for the methanolysis of $PhSiH_3$ with catalyst **1** with and without $LiHBEt_3$ under different methanol concentrations. Reaction conditions: 1 mol% of **1**, 1 mol% of $LiHBEt_3$ (when required), 0.5 mmol of $PhSiH_3$, at 50 °C.

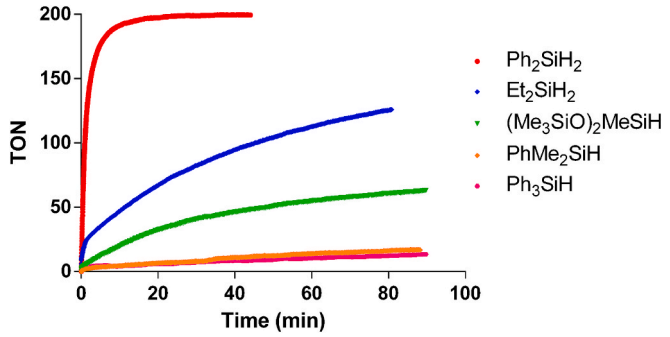

Fig. 11. Conversion over time for the methanolysis of different silanes with catalyst **1**. Reaction conditions: 1 mol% of **1**, 1 mol% of $LiHBEt_3$, 0.5 mmol of silane, 0.5 mL of a 4:1 mixture MeOH:THF at 50 °C.

tube. Upon heating the solution at 50 °C for 1 h, a doublet appeared at δ –5.50 ppm with a H-P coupling constant of 53 Hz in the ^{1}H NMR spectrum, consistent with the formation of the Mn-hydride active species (Fig. S43). The ^{31}P NMR spectrum displays two resonances: one sharp peak attributable to the unreacted starting material, and a broad signal at 39.1 ppm corresponding to hydride, which is the main species in solution (Fig. S44).

2.3. Computational study of the reaction mechanism

In order to shed light on the reaction mechanism, we conducted a detailed computational study based on Density Functional Theory (DFT), as explained in the Computational Details section. Given that experimental evidence indicates that $LiHBEt_3$ facilitates the formation of Mn–hydride species, thereby enhancing catalytic activity, we considered the hydride derivative of **1** to be the active species under these conditions and considered it as the starting point of the catalytic cycle. For the sake of clarity and to avoid any potential confusion with experimentally prepared and characterized species, we designated this species as **A**, using subsequent capital letters to denote other reaction intermediates. The reaction profile corresponding to the proposed mechanism for the reaction between $PhSiH_3$ and methanol, leading to the formation of $H_2SiPh(OMe)$, is shown in Fig. 12.

The first step involves decoordination of the triazole-based ligand, which is essential for the formation of intermediate **B** through coordination of a hydrosilane molecule. Note that intermediate **B** lies only 1.5 kcal·mol^{-1} higher in Gibbs energy than **A**. It is worth mentioning that the η^3-H_2SiR_3 coordination mode in **B** has been previously reported and experimentally characterized [47–49]. Subsequently, hydrosilane methoxylation occurs directly via $\mathbf{TS_{BC}}$ through a concerted process in which the Si–O bond in the newly formed alcoxysilane the H–H bond in H_2, and a new Mn–H bond are generated at the expense of the O–H bond in methanol, the Si–H bond in the hydrosilane, and the pre-existing Mn–H bond (see Fig. 13). This concerted reaction mechanism is strongly related to a previous one recently reported by us for the same chemical process catalysed by a Co(I) complex [46], as well as that described by other authors for the Ru complex [TpRu(PPh$_3$)(η^3-$H_2SiEtMe_2$)] [48]. Such a process requires to surmount a Gibbs energy barrier of 13.9 kcal·mol^{-1} (dictated by the Gibbs energy difference between $\mathbf{TS_{BC}}$ and **A**). As a result, the dihydrogen complex **C** forms with concomitant release of the $Ph(OMe)SiH_2$ product. This intermediate lies at a relative Gibbs energy of –9.0 kcal·mol^{-1}, reflecting the high thermodynamic favourability of the preceding step. Finally, the coordinated H_2 molecule is released, followed by coordination of the labile nitrogen

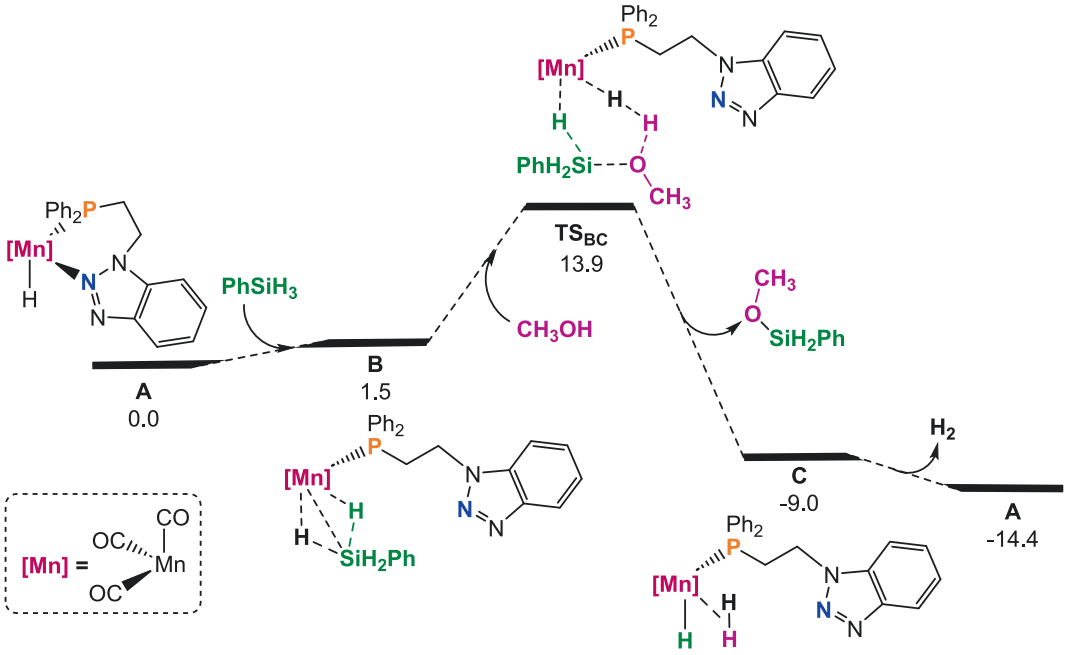

Fig. 12. DFT calculated Gibbs free energy profile (in kcal·mol^{-1}, relative to **A** and the isolated molecules) for the methanolysis of $PhSiH_3$ via a concerted reaction pathway.

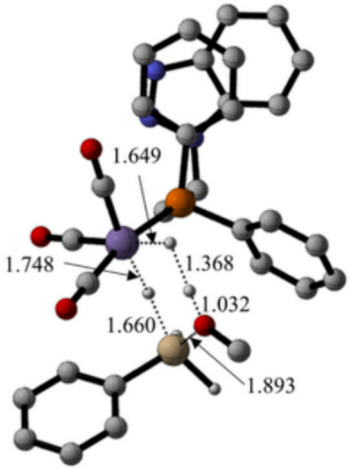

Fig. 13. Geometrical representation of the structure of $\mathbf{TS_{BC}}$. Key distances are provided in Å. Non-essential hydrogen atoms have been omitted for clarity.

atom of the triazole-based ligand scaffold, thereby regenerating the original species **A**.

At this point, it is worth noting that an alternative stepwise reaction mechanism was also considered, as shown in Fig. 14. In line with the mechanism described above, the process begins with a ligand exchange between the triazole-based fragment and the hydrosilane, affording intermediate **B**. Subsequently, an H_2 molecule and a Mn–Si bond are formed via a metal-assisted σ-bond metathesis process [50] as dictated by $\mathbf{TS_{BD}}$ (Fig. 15a). This transition state lies at a relative Gibbs free energy of only 9.6 kcal·mol^{-1}. As a result, Mn-silyl intermediate **D**, which bears a coordinated H_2 molecule is obtained, has a relative Gibbs energy of 8.0 kcal·mol^{-1}. The final step involves formation of the Si—O bond in the product, occurring concurrently with the deprotonation of the methanol molecule. This transformation proceeds via $\mathbf{TS_{DA}}$, which has a relative Gibbs free energy of 19.4 kcal·mol^{-1}, and features a significant interaction between a non-reactive hydrogen atom of the silyl group and the Mn centre (see Fig. 15b), in line with the coordination mode explained for intermediate **B**.

Overall, this reaction pathway exhibits an effective energy span of 19.4 kcal·mol^{-1} (Gibbs energy difference between $\mathbf{TS_{DA}}$ and **A**) [51], which is 5.5 kcal·mol^{-1} higher in Gibbs free energy than the concerted mechanism depicted in Fig. 12, with an energy span of 13.9 kcal·mol^{-1} (Gibbs energy difference between $\mathbf{TS_{BC}}$ and **A**). Consequently, since all elementary steps in the stepwise pathway shown in Fig. 14 are reversible—except for the final step, whose reverse process has a Gibbs energy barrier of 33.8 kcal·mol^{-1}—the reaction landscape is expected to be dominated by the concerted alternative.

The pronounced increase in catalytic activity upon addition of LiHBEt$_3$ plausibly arises from access to a more favourable reaction pathway enabled by the formation of a hydride species, which constitutes the above explained reaction mechanism. In the absence of LiHBEt$_3$, the reaction likely follows an alternative pathway. Based on previous reports and our experimental observations, especially the lack of an induction period, which suggests the absence of a catalyst activation step; we propose that the process is consistent with a Luo–Crabtree-type mechanism [4]. This pathway would involve (i) hydride abstraction from the hydrosilane, yielding a Mn-hydride intermediate and [R$_3$Si–O(H)CH$_3$]$^+$, followed by (ii) hydride protonation by this intermediate to produce H_2 and R$_3$Si–OCH$_3$. Higher energies for these types of mechanism, compared to concerted pathways, have been previously reported.

To test this hypothesis, complex **1** was reacted with three equivalents of PhSiH$_3$ in THF-d$_8$ in a Young NMR tube at 50 °C and monitored over 5 h; however, no hydride formation was observed in the ^{1}H NMR spectra. Upon addition of methanol to the reaction mixture, hydrogen evolution was detected, but no signals appeared in the hydride region. These observations suggest that the formation of two distinct active species gives rise to divergent reaction pathways, accounting for the different reactivity observed in the presence or absence of LiHBEt$_3$.

3. Experimental

All experiments were carried out under an inert atmosphere using the Schlenk technique. The complexes were stored depending on their stability under an inert atmosphere or in a MBraun dry box. The solvents were previously dried and distilled under argon or by means of a solvent

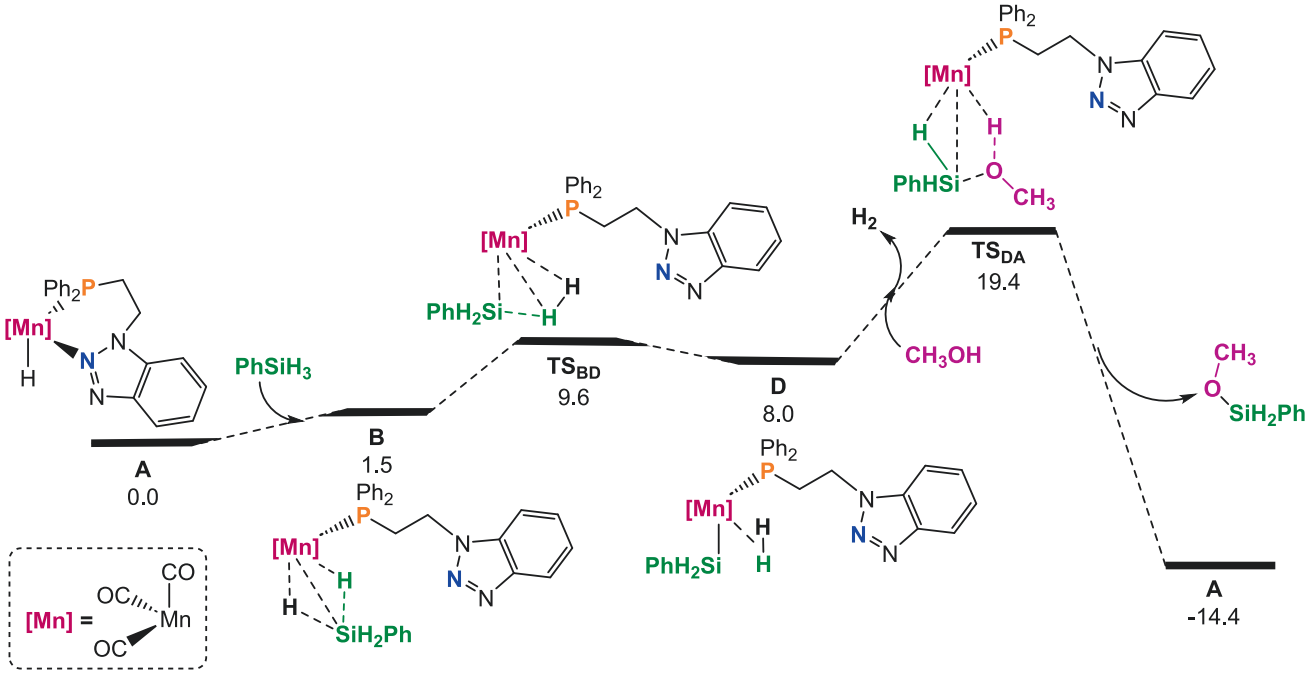

Fig. 14. DFT calculated Gibbs free energy profile (in kcal·mol^{-1}, relative to **A** and the isolated molecules) for the methanolysis of PhSiH$_3$ via a stepwise reaction pathway.

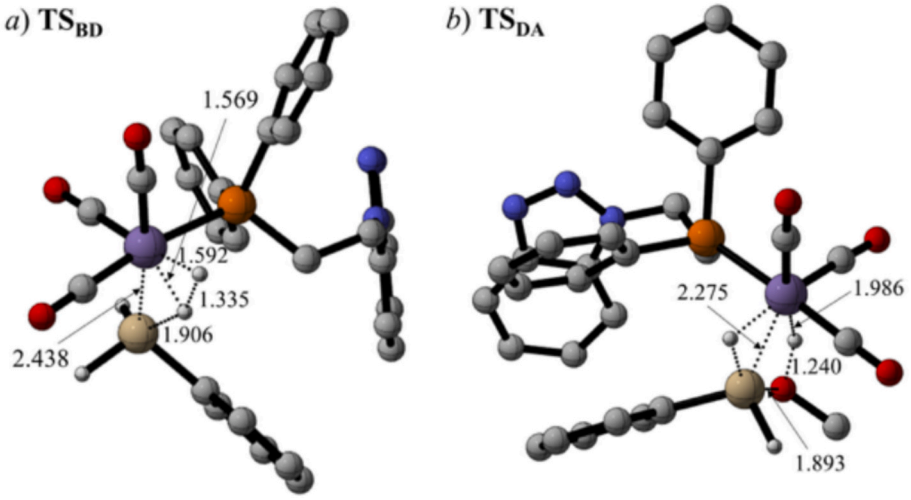

Fig. 15. Geometrical representation of the geometrical structure of *a*) **TS$_{BD}$** and *b*) **TS$_{DA}$**. Key distances are provided in Å. Non-essential hydrogen atoms have been omitted for clarity.

purification system (SPS) and collected in an inert atmosphere. All other commercially available starting materials were purchased from Merck and were used without further purification. The NMR spectra were recorded at 298 K in the Bruker Avance 300 MHz, Bruker ARX 300 MHz and Bruker Avance 400 MHz spectrometers. Chemical shifts are expressed in ppm and the residual peaks of the solvent were taken as reference. Coupling constants J are given in Hz. Spectral assignments were achieved by combination of ^{1}H–^{1}H COSY, ^{13}C APT, ^{1}H–^{13}C HSQC and ^{1}H–^{13}C HMBC experiments. Attenuated total reflection infrared spectra (ATR-IR) of solid samples were run on a PerkinElmer Spectrum 100 FT-IR spectrometer. High-resolution electrospray mass spectra (HRMS) were acquired using a Bruker MicroTOF-Q hybrid quadrupole time-of-flight spectrometer. Ligands 1-(2-(diphenylphosphanyl)ethyl)-1*H*-benzo-1,2,3-triazole (**L1**), 2-(2-(diphenylphosphanyl)ethyl)–2*H*-benzo-1,2,3-triazole (**L2**) [35], and 1-((diphenylphosphanyl)methyl)-1H-benzo-1,2,3-triazole (**L3**) [32] were synthesized according to preparations previously described in literature.

Synthesis of 1. The complex [MnBr(CO)$_5$] (124 mg, 0.45 mmol) was dissolved in acetonitrile (7 mL), 1-(2-(diphenylphosphanyl)ethyl)-1*H*-benzo-1,2,3-triazole (150 mg, 0.45 mmol) was added and it was stirred for 1 h at 80 °C. After that, AgBF$_4$ (88 mg, 0.45 mmol) was added and was stirred for 24 h protected from light. The mixture was filtered through Celite®, the solvent was evaporated under reduced pressure and the resulting pale-yellow oil was washed with hexane (3 x 10 mL) to afford the title complex as a pale-yellow solid (226 mg, 0.38 mmol, 84 % yield). ^{1}H NMR (CD$_3$CN, 400 MHz): δ 8.04 (d, $^{3}J_{H-H}$ = 8.5, 1H, C*H*$_{Ar}$), 7.81 (d, $^{3}J_{H-H}$ = 8.6, 1H, C*H*$_{Ar}$), 7.76–7.65 (m, 5H, PC*H*$_{Ar}$ + C*H*$_{Ar}$), 7.57–7.51 (m, 7H, PC*H*$_{Ar}$ + C*H*$_{Ar}$), 5.09–4.83 (m, 2H, NC*H*$_2$), 3.31–3.14 (m, 2H, C*H*$_2$P). ^{13}C{^{1}H} NMR APT, ^{1}H–^{13}C HSQC, ^{1}H–^{13}C HMBC (CD$_3$CN, 101 MHz): δ 146.2 (s, *C*$_{ipso}$N), 136.9 (s, *C*$_{ipso}$N), 133.2 (d, J_{P-C} = 9.4, *C*$_{Ar}$P), 132.9 (d, J_{P-C} = 10.0, *C*$_{Ar}$P), 132.6 (d, J_{P-C} = 2.4, *C*$_{Ar}$P), 132.6 (d, $^{1}J_{P-C}$ = 47.5, *C*$_{ipso}$P), 132.4 (d, J_{P-C} = 2.6, *C*$_{Ar}$P), 131.0 (d, $^{1}J_{P-C}$ = 40.5, *C*$_{ipso}$P), 130.7 (s, *C*$_{Ar}$N), 130.5 (d, J_{P-C} = 10.0, *C*$_{Ar}$P), 130.4 (d, J_{P-C} = 9.8, *C*$_{Ar}$P), 127.4 (s, *C*$_{Ar}$N), 119.7 (s, *C*$_{Ar}$N), 111.4 (s, *C*$_{Ar}$N), 44.7 (d, $^{2}J_{P-C}$ = 3.5, NC*H*$_2$), 23.8 (d, $^{1}J_{P-C}$ = 21.9, *C*H$_2$P), (CO and NCCH$_3$ not observed). ^{31}P{^{1}H} NMR (CD$_3$CN, 162 MHz): δ 41.5 (bs, PPh$_2$). IR (cm^{-1}, pure sample) 2045, 1974, 1939 (Mn–*CO*), 1052 (BF$_4$). HRMS (ESI) Calcd for [C$_{25}$H$_{21}$MnN$_4$O$_3$P]$^{+}$ 511.0732, found 511.0713. Calcd for [C$_{23}$H$_{18}$MnN$_3$O$_3$P]$^{+}$ 470.0466, found 470.0542. Calcd for [C$_{20}$H$_{18}$MnN$_3$P]$^{+}$ 386.0619, found 386.0719.

Synthesis of 2. The complex [MnBr(CO)$_5$] (83 mg, 0.30 mmol) was dissolved in acetonitrile (5 mL), 2-(2-(diphenylphosphanyl)ethyl)–2*H*-benzo-1,2,3-triazole (100 mg, 0.30 mmol) was added and it was stirred for 1 h at 80 °C. After that, AgBF$_4$ (59 mg, 0.30 mmol) was added and was stirred for 24 h protected from light. The mixture was filtered through Celite®, the solvent was evaporated under reduced pressure and the resulting pale-yellow oil was washed with hexane (3 x 10 mL) to afford the title complex as a pale-yellow solid (161 mg, 0.27 mmol, 90 % yield). ^{1}H NMR (CD$_3$CN, 400 MHz): δ 8.36–7.05 (m, 14H, PC*H*$_{Ar}$ + C*H*$_{Ar}$), 5.49–4.68 (m, 2H, NC*H*$_2$), 3.47–2.78 (m, 2H, C*H*$_2$P). ^{13}C{^{1}H} NMR APT, ^{1}H–^{13}C HSQC, ^{1}H–^{13}C HMBC (CD$_3$CN, 101 MHz): Major isomer, δ 147.8 (s, *C*$_{ipso}$N), 144.8 (s, *C*$_{ipso}$N), 133.3 (d, J_{P-C} = 10.0, *C*$_{Ar}$P), 133.1 (d, J_{P-C} = 9.2, *C*$_{Ar}$P), 132.8 (d, J_{P-C} = 2.6, *C*$_{Ar}$P), 132.4 (d, $^{1}J_{P-C}$ = 47.1, *C*$_{ipso}$P), 132.3 (d, J_{P-C} = 2.6, *C*$_{Ar}$P), 130.9 (d, $^{1}J_{P-C}$ = 41.2, *C*$_{ipso}$P), 130.9 (s, *C*$_{Ar}$N), 130.5 (d, J_{P-C} = 10.0, *C*$_{Ar}$P), 130.3 (d, J_{P-C} = 9.8, *C*$_{Ar}$P), 128.9 (s, *C*$_{Ar}$N), 120.7 (s, *C*$_{Ar}$N), 117.8 (s, *C*$_{Ar}$N), 53.9 (d, $^{2}J_{P-C}$ = 1.9, NC*H*$_2$), 25.4 (d, $^{1}J_{P-C}$ = 22.1, *C*H$_2$P), (CO and NCCH$_3$ not observed). ^{31}P{^{1}H} NMR (CD$_3$CN, 162 MHz): Major isomer, δ 43.5 (bs, PPh$_2$). IR (cm^{-1}, pure sample) 2043, 1935, 1883 (Mn–*CO*), 1051 (BF$_4$). HRMS (ESI) Calcd for [C$_{25}$H$_{21}$MnN$_4$O$_3$P]$^{+}$ 514.0920, found 514.0924. Calcd for [C$_{23}$H$_{18}$MnN$_3$O$_3$P]$^{+}$ 470.0466, found 470.0514. Calcd for [C$_{20}$H$_{18}$MnN$_3$P]$^{+}$ 386.0619, found 386.0685.

Synthesis of 3. The complex [MnBr(CO)$_5$] (56 mg, 0.20 mmol) was dissolved in acetonitrile (5 mL), 1-((diphenylphosphanyl)methyl)-1*H*-benzo-1,2,3-triazole (65 mg, 0.20 mmol) was added and it was stirred for 1 h at 80 °C. After that, the solvent was evaporated under reduced pressure and the resulting yellow oil was washed with hexane (3 x 5 mL) to afford the title complex as a yellow solid (96.7 mg, 0.18 mmol, 88 % yield). ^{1}H NMR (CD$_3$CN, 400 MHz): δ 8.13–8.02 (m, 3H, C*H*$_{Ar}$), 7.86–7.80 (m, 1H, C*H*$_{Ar}$), 7.76–7.70 (m, 1H, C*H*$_{Ar}$), 7.67–7.55 (m, 4H, C*H*$_{Ar}$ + PC*H*$_{Ar}$), 7.45–7.34 (m, 3H, PC*H*$_{Ar}$), 7.28–7.20 (m, 2H, PC*H*$_{Ar}$), 5.99 (at, ^{2}J = 12.6, 1H, C*H*$_2$P), 5.23 (ad, $^{2}J_{H-H}$ = 13.2, 1H, C*H*$_2$P). ^{13}C{^{1}H} NMR APT, ^{1}H–^{13}C HSQC, ^{1}H–^{13}C HMBC (CD$_3$CN, 101 MHz): δ 147.9 (s, *C*$_{ipso}$N), 135.6 (d, $^{1}J_{P-C}$ = 40.2, *C*$_{ipso}$P), 135.5 (d, J_{P-C} = 10.1, *C*$_{Ar}$P), 135.2 (d, $^{3}J_{P-C}$ = 5.4, *C*$_{ipso}$N), 133.1 (d, J_{P-C} = 2.4, *C*$_{Ar}$P), 131.7 (d, J_{P-C} = 2.2, *C*$_{Ar}$P), 131.2 (d, J_{P-C} = 10.7, *C*$_{Ar}$P), 130.6 (s, *C*$_{Ar}$N), 130.2 (d, J_{P-C} = 1.8, *C*$_{Ar}$P), 130.1 (d, J_{P-C} = 0.8, *C*$_{Ar}$P), 128.6 (d, $^{1}J_{P-C}$ = 47.9, *C*$_{ipso}$P), 127.1 (s, *C*$_{Ar}$N), 119.8 (s, *C*$_{Ar}$N), 111.9 (s, *C*$_{Ar}$N), 49.6 (d, $^{1}J_{P-C}$ = 25.8, *C*H$_2$P), (CO not observed). ^{31}P{^{1}H} NMR (CD$_3$CN, 162 MHz): δ 65.2 (bs, PPh$_2$). IR (cm^{-1}, pure sample) 2028, 1952, 1920 (Mn–*CO*). HRMS (ESI) Calcd for [C$_{22}$H$_{16}$BrMnN$_3$NaO$_3$P]$^{+}$ 557.9397, found 557.9385.

Synthesis of 4. The complex **3** (85 mg, 0.16 mmol) was dissolved in acetonitrile (5 mL), AgBF$_4$ (31 mg, 0.16 mmol) was added and was stirred for 24 h protected from light. The mixture was filtered through Celite®, the solvent was evaporated under reduced pressure and the resulting pale-yellow oil was washed with hexane (3 x 5 mL) to afford the title complex as a pale-yellow solid (76 mg, 0.13 mmol, 83 % yield).

^{1}H NMR (CD_3CN, 400 MHz): δ 8.07 (d, $^3J_{H–H}$ = 8.5, 1H, CH_{Ar}), 7.90 (d, $^3J_{H–H}$ = 8.5, 1H, CH_{Ar}), 7.76 (at, $^3J_{H–H}$ = 7.7, 1H, CH_{Ar}), 7.73–7.65 (m, 2H, PCH_{Ar}), 7.61–7.50 (m, 9H, PCH_{Ar} + CH_{Ar}), 5.77 (dd, $^2J_{H–H}$ = 15.0, $^3J_{P–H}$ = 7.2, 1H, CH_2P), 5.52 (dd, $^2J_{H–H}$ = 15.0, $^3J_{P–H}$ = 5.8, 1H, CH_2P), 1.65 (s, 3H, NCCH_3). ^{13}C{^{1}H} NMR APT, ^{1}H–^{13}C HSQC, ^{1}H–^{13}C HMBC (CD_3CN, 101 MHz): δ 148.2 (s, C_{ipso}N), 135.7 (d, $^3J_{P-C}$ = 5.7, C_{ipso}N), 133.3 (d, J_{P-C} = 2.6, C_{Ar}P), 133.2 (d, J_{P-C} = 11.2, C_{Ar}P), 132.9 (d, J_{P-C} = 10.9, C_{Ar}P), 132.9 (d, J_{P-C} = 2.4, C_{Ar}P), 131.9 (bs, N*C*CH$_3$), 131.1 (s, C_{Ar}N), 130.6 (d, J_{P-C} = 10.8, C_{Ar}P), 130.5 (d, J_{P-C} = 10.8, C_{Ar}P), 130.1 (d, $^1J_{P–C}$ = 50.5, C_{ipso}P), 128.6 (d, $^1J_{P–C}$ = 42.8, C_{ipso}P), 127.4 (s, C_{Ar}N), 119.9 (s, C_{Ar}N), 112.1 (s, C_{Ar}N), 48.6 (d, $^1J_{P–C}$ = 26.2, *C*H$_2$P), 3.9 (s, NCCH$_3$) (CO not observed). ^{31}P{^{1}H} NMR (CD_3CN, 162 MHz): δ 71.6 (bs, PPh_2). ^{19}F NMR (CD_3CN, 282 MHz): δ −151.4 (bs, BF_4). IR (cm^{-1}, pure sample) 2049, 1971, 1949 (Mn–*CO*), 1019 (BF_4). HRMS (ESI) Calcd for $[C_{24}H_{19}MnN_4O_3P]^+$ 497.0575, found 497.0549. Calcd for $[C_{22}H_{16}MnN_3O_3P]^+$ 456.0310, found 456.0303. Calcd for $[C_{19}H_{16}MnN_3P]^+$ 372.0462, found 372.0460.

Synthesis of 5. To a solution of [MnBr(CO)$_5$] (43 mg, 0.16 mmol) in acetonitrile (7 mL) were added 2 equivalents of **L3** (100 mg, 0.32 mmol), and the resulting mixture was stirred for 24 h at 80 °C. Subsequently, $AgBF_4$ (31 mg, 0.16 mmol) was added, and the mixture was stirred for 24 h at room temperature while being protected from light. The reaction mixture was then filtered through Celite®, the solvent was evaporated under reduced pressure, and the resulting pale-yellow oil was washed with hexane (3 × 10 mL), affording the title compound as a yellow powder in 90 % yield (120 mg, 0.14 mmol). ^{1}H NMR (CD_3CN, 400 MHz): δ 7.82–7.79 (m, 2H, CH_{Ar}), 7.67–7.62 (m, 3H, PCH_{Ar}), 7.61–7.53 (m, 13H, PCH_{Ar} + CH_{Ar}), 7.49–7.34 (m, 10*H*, PCH_{Ar} + CH_{Ar}), 5.82–5.68 (m, 4H, PCH_{Ar} + CH_{Ar}). ^{13}C{^{1}H} NMR APT, ^{1}H–^{13}C HSQC, ^{1}H–^{13}C HMBC (CD_3CN, 101 MHz): δ 147.2 (s, C_{ipso}N), 135.1 (at, J_{P-C} = 2.6, C_{ipso}N), 134.7 (d, $^1J_{P–C}$ = 47.7, C_{ipso}P), 134.4 (at, J_{P-C} = 5.6, C_{Ar}P), 132.4 (at, J_{P-C} = 5.0, C_{Ar}P), 132.4 (at, J_{P-C} = 5.2, C_{Ar}P), 131.5 (d, $^1J_{P–C}$ = 42.5, C_{ipso}P), 131.0 (s, C_{Ar}N), 130.4 (at, J_{P-C} = 5.0, C_{Ar}P), 129.9 (at, J_{P-C} = 5.2, C_{Ar}P), 127.0 (s, C_{Ar}N), 119.8 (s, C_{Ar}N), 111.9 (s, C_{Ar}N), 49.3 (dd, $J_{P–C}$ = 12.1, 10.8, *C*H$_2$P) (CO not observed). ^{31}P{^{1}H} NMR (CD_3CN, 162 MHz): δ 84.4 (bs, PPh_2). ^{19}F NMR (CD_3CN, 282 MHz): δ − 151.8 (bs, BF_4). IR (cm^{-1}, ATR): 1953, 1890 (Mn–*CO*), 1031 (BF_4). HRMS (ESI$^+$) *m/z* Calc. for $[C_{40}H_{32}MnN_6O_2P_2]^+$ 745.1442, found 745.1437.

General protocol for the methanolysis and hydrolysis reactions. The catalyst (0.005 mmol, 1 mol%) was dissolved in a mixture of THF (0.25 mL) and methanol or water (0.25 mL) in the reactor and equipped with a magnetic stir bar. The mixture was placed in an oil bath at 50 °C. Once the pressure stabilized, the silane (0.50 mmol) was added to the reaction mixture with a microsyringe under inert atmosphere. The gas formation was measured using a Man on the Moon series X102 kit microreactor. The amount of gas (H_2) produced during the reaction was calculated using the Ideal Gas Law.

NOTE: To generate the hydride in situ, a 1 M solution of $LiHBEt_3$ in THF (0.005 mmol, 1 mol%, 5 μL) was added to a solution of the catalyst (0.005 mmol, 1 mol%) in THF (0.25 mL) under an inert atmosphere. Then, 0.25 mL of methanol or water is added, and the resulting mixture placed in an oil bath at 50 °C. Once the temperature has stabilized, the silane (0.5 mmol) is added using a microsyringe.

X-ray diffraction analysis. Single crystals of [MnBr(CO)$_3$**L1**], **2**, **4** and **5** were collected at 100(2) K on a Bruker D8 VENTURE diffractometer using graphite-monochromated Mo-Kα radiation (λ = 0.71073 Å). For **3**, X-ray diffraction data were collected at 100(2) K on an MD2M-Maatel diffractometer in XALOC beamline at ALBA synchrotron (Spain) with a wavelength of 0.72940 Å, using a Dectris Pilatus 6 M detector positioned 122.1 mm from the crystal. Intensities were integrated and corrected for absorption effects with the SAINT-PLUS [52] and SADABS [53], both included in the APEX3 and APEX4 packages. The structures were solved with SHELXS [54] and refined by full matrix least-squares on F^2 with SHELXL [55] under WinGX [56] or Olex2 [56] packages. Further details on the refinement are reported in Supporting Information.

Computational Details. DFT calculations were performed by using the Gaussian16 software package [57]. The reaction mechanisms were obtained on the basis of the M06-L exchange–correlation functional [58], which is based on its established efficacy in characterizing spin states in first-row transition metals, as well as in catalytic processes involving Mn centres, and accounts for dispersion corrections [32,59–63]. Geometry optimizations and frequency calculations were carried out with the def2-SVP basis set, electronic energies being further refined through single point calculations with the triple-zeta def2-TZVP basis set [64]. In all calculations, the *"ultrafine"* integration grid was employed. Solvent corrections for tetrahydrofuran, which were included in energies and gradient calculations, were accounted for by means of the we considered the Solvation Model based on Density (SMD) [65]. We note that, while the highest catalytic activities were experimentally observed in a MeOH/THF mixture, we consider that the SMD model in THF provides a sufficiently accurate description of solvent effects, particularly considering the implicit nature of the model.

Intermediates and transition states were optimized assuming a singlet ground state for the Mn centre. This is consistent with a formal + I oxidation state (d^6 electronic configuration) in an octahedral geometry and the presence of three CO ligands in A, which are well-known being strong-field ligands that favour a low-spin singlet state. Indeed, singlet state have been generally assumed in related systems [36,39,42]. Anyway, to assess the possible relevance of triplet states, we performed wave function stability analyses on the singlet configurations. All structures were found to be stable, and thus only the singlet states were considered. Note that although the geometries of singlet and triplet states may differ slightly, they are expected to be broadly similar, and such geometric variations are not anticipated to significantly affect the results.

The nature of all stationary points was verified through analytical frequency analyses at the def2-SVP level of theory. These calculations were also used to obtain Gibbs energy corrections at 298.15 K. The translational entropy contribution was removed following the procedure proposed by Morokuma and co-workers [66]. CylView software was used for structure graphical representations [67].

4. Conclusions

This study demonstrates that triazole-based P-N ligands offer a powerful strategy to tune the reactivity of Mn(I) carbonyl catalysts through controlled hemilability. Complexes incorporating more labile triazole donors exhibit markedly enhanced activities, reaching turnover frequencies above 45,000 h^{-1} in the methanolysis of hydrosilanes upon formation of the Mn-hydride active species by reaction of **1** with $LiHBEt_3$.

DFT studies support a concerted reaction pathway that necessitates the formation of a hydride active species and transient triazole dissociation. These insights highlight how reversible metal–ligand coordination can be leveraged to balance activity and stability in Earth-abundant metal catalysis.

Overall, these results position hemilabile triazole-based P-N ligands as robust and tuneable scaffolds to fine-tune Mn(I) catalysts, highlighting their potential for Si–O bond formation and hydrogen generation.

CRediT authorship contribution statement

Susana García-Abellán: Methodology, Investigation, Formal analysis, Data curation, Conceptualization. **Jorge Gonzalo:** Investigation. **Andrea Pérez-García:** Investigation. **Miguel A. Casado:** Investigation, Formal analysis. **Pilar García-Orduña:** Formal analysis, Data curation. **Vincenzo Passarelli:** Formal analysis, Data curation. **Julen Munárriz:** Writing – review & editing, Supervision, Methodology, Conceptualization. **Manuel Iglesias:** Writing – review & editing, Writing – original draft, Supervision, Methodology, Funding acquisition, Conceptualization.

Declaration of competing interest

The authors declare that they have no known competing financial interests or personal relationships that could have appeared to influence the work reported in this paper.

Acknowledgements

The authors acknowledge the Ministerio de Ciencia, Innovación y Universidades (Grant No. PID2024-159030NA-I00 and PID2021-126212OB-I00), and Departamento de Educación, Ciencia y Universidades del Gobierno de Aragón (group E42_23R). The authors also thank the Servicio General de Apoyo a la Investigación – SAI of the Universidad de Zaragoza and the ISQCH/CEQMA (CSIC) for technical support and facilities, as well as the Instituto de Biocomputación y Física de Sistemas Complejos (BIFI, Universidad de Zaragoza) for providing computational resources.

Appendix A. Supplementary data

Supplementary data to this article can be found online at https://doi.org/10.1016/j.jcat.2026.116954.

Data availability

The research data is available as Supporting Information

References

[1] J. Chen, M. McGraw, E.-Y.-X. Chen, Diverse catalytic systems and mechanistic pathways for hydrosilylative reduction of CO_2, ChemSusChem 12 (2019) 4543–4569, https://doi.org/10.1002/cssc.201901764.
[2] A. Sinopoli, N.T. La Porte, J.F. Martinez, M.R. Wasielewski, M. Sohail, Manganese carbonyl complexes for CO2 reduction, Coord. Chem. Rev. 365 (2018) 60–74, https://doi.org/10.1016/j.ccr.2018.03.011.
[3] K. Das, S. Waiba, A. Jana, B. Maji, Manganese-catalyzed hydrogenation, dehydrogenation, and hydroelementation reactions, Chem. Soc. Rev. 51 (2022) 4386–4464, https://doi.org/10.1039/D2CS00093H.
[4] A. Luque-Gómez, M. Iglesias, Earth-abundant metal complexes as catalysts for the dehydrogenative coupling of hydrosilanes and alcohols, Eur. J. Org. Chem. 28 (2025) e202500215, https://doi.org/10.1002/ejoc.202500215.
[5] V. Chandrasekhar, R. Boomishankar, S. Nagendran, Recent developments in the synthesis and structure of organosilanols, Chem. Rev. 104 (2004) 5847–5910, https://doi.org/10.1021/cr0306135.
[6] I. Ojima, Z. Li, J. Zhu, Recent Advances in the Hydrosilylation and Related Reactions, in: Z. Rappoport, Y. Apeloig (Eds.), PATAI'S Chemistry of Functional Groups, 1st ed., Wiley, 1998: pp. 1687–1792. Doi: 10.1002/0470857250.ch29.
[7] T. Li, H. Zhang, A.S.C. Chan, S.-S. Meng, Manganese-catalyzed dehydrogenative coupling of silanes and hydroxyl compound controlled by phosphine oxide, Cell Rep. Phys. Sci. 4 (2023) 101313, https://doi.org/10.1016/j.xcrp.2023.101313.
[8] E. Antico, M. Leutzsch, N. Wessel, T. Weyhermüller, C. Werlé, W. Leitner, Selective oxidation of silanes into silanols with water using $[MnBr(CO)_5]$ as a precatalyst, Chem. Sci. 14 (2023) 54–60, https://doi.org/10.1039/D2SC05959B.
[9] H.S. Hilal, S. Khalaf, M. Al Nuri, M. Karmi, Homogeneous catalysis of the reaction of silanes with alcohols using decacarbonyl dimanganese (0), J. Mol. Catal. 35 (1986) 137–142, https://doi.org/10.1016/0304-5102(86)87019-5.
[10] B.T. Gregg, A.R. Cutler, Manganese carbonyl bromide-catalyzed alcoholysis of the monohydrosilane HSiMe2Ph, Organometallics 13 (1994) 1039–1043, https://doi.org/10.1021/om00015a043.
[11] C.N. Scott, C.S. Wilcox, A Mild synthesis of unsymmetrical bisalkoxysilanes through catalyzed alcoholysis of hydridosilanes containing C−C multiple bonds and aryl halides, J. Org. Chem. 75 (2010) 253–256, https://doi.org/10.1021/jo9022765.
[12] X. Fang, J. Huhmann-Vincent, B.L. Scott, G.J. Kubas, H2 binding to and silane alcoholysis on an electrophilic Mn(I) fragment with tied-back phosphite ligands. X-ray structure of a Mn–CH2Cl2 complex, J. Organomet. Chem. 609 (2000) 95–103, https://doi.org/10.1016/S0022-328X(00)00230-8.
[13] S. Vijjamarri, V.K. Chidara, J. Rousova, G. Du, Dehydrogenative coupling of alcohols and carboxylic acids with hydrosilanes catalyzed by a salen–Mn(v) complex, Catal. Sci. Technol. 6 (2016) 3886–3892, https://doi.org/10.1039/C5CY01912E.
[14] S. Vijjamarri, M. Hull, E. Kolodka, G. Du, Renewable isohexide-based, hydrolytically degradable poly(silyl ether)s with high thermal stability, ChemSusChem 11 (2018) 2881–2888, https://doi.org/10.1002/cssc.201801123.
[15] X. Ma, Z. Zuo, G. Liu, Z. Huang, Manganese-catalyzed asymmetric hydrosilylation of aryl ketones, ACS Omega 2 (2017) 4688–4692, https://doi.org/10.1021/acsomega.7b00713.
[16] S. Vijjamarri, S. Streed, E.M. Serum, M.P. Sibi, G. Du, Polymers from bioderived resources: synthesis of poly(silylether)s from furan derivatives catalyzed by a salen–Mn(V) complex, ACS Sustain. Chem. Eng. 6 (2018) 2491–2497, https://doi.org/10.1021/acssuschemeng.7b03932.
[17] W.-S. Han, T.-J. Kim, S.-K. Kim, Y. Kim, Y. Kim, S.-W. Nam, S.O. Kang, Silane-based hydrogen storage materials for fuel cell application: hydrogen release via methanolysis and regeneration by hydride reduction from organosilanes, Int. J. Hydrogen Energy 36 (2011) 12305–12312, https://doi.org/10.1016/j.ijhydene.2011.06.118.
[18] B. Schulze, U.S. Schubert, Beyond click chemistry – supramolecular interactions of 1,2,3-triazoles, Chem. Soc. Rev. 43 (2014) 2522, https://doi.org/10.1039/c3cs60386e.
[19] J.D. Crowley, P.H. Bandeen, A multicomponent CuAAC "click" approach to a library of hybrid polydentate 2-pyridyl-1,2,3-triazole ligands: new building blocks for the generation of metallosupramolecular architectures, Dalton Trans. 39 (2010) 612–623, https://doi.org/10.1039/B911276F.
[20] E. Kitteringham, Z. Zhou, B. Twamley, D.M. Griffith, Au(III) and Pt(II) complexes of a novel and versatile 1,4-disubstituted 1,2,3-triazole-based ligand possessing diverse secondary and tertiary coordinating groups, Inorg. Chem. 57 (2018) 12282–12290, https://doi.org/10.1021/acs.inorgchem.8b01994.
[21] K.Q. Vuong, M.G. Timerbulatova, M.B. Peterson, M. Bhadbhade, B.A. Messerle, Cationic Rh and Ir complexes containing bidentate imidazolylidene–1,2,3-triazole donor ligands: synthesis and preliminary catalytic studies, Dalton Trans. 42 (2013) 14298, https://doi.org/10.1039/c3dt51440d.
[22] G.F. Manbeck, W.W. Brennessel, C.M. Evans, R. Eisenberg, Tetranuclear copper(I) iodide complexes of chelating bis(1-benzyl-1 *H* -1,2,3-triazole) ligands: structural characterization and solid state photoluminescence, Inorg. Chem. 49 (2010) 2834–2843, https://doi.org/10.1021/ic902236n.
[23] H. Struthers, T.L. Mindt, R. Schibli, Metal chelating systems synthesized using the copper(i) catalyzed azide-alkynecycloaddition, Dalton Trans. 39 (2010) 675–696, https://doi.org/10.1039/B912608B.
[24] S. Bai, D.J. Young, T.S.A. Hor, Nitrogen-rich azoles as ligand spacers in coordination polymers, Chem. Asian J. 6 (2011) 292–304, https://doi.org/10.1002/asia.201000698.
[25] T.L. Mindt, H. Struthers, L. Brans, T. Anguelov, C. Schweinsberg, V. Maes, D. Tourwé, R. Schibli, "Click to Chelate": synthesis and installation of metal chelates into biomolecules in a single step, J. Am. Chem. Soc. 128 (2006) 15096–15097, https://doi.org/10.1021/ja066779f.
[26] D. Urankar, B. Pinter, A. Pevec, F. De Proft, I. Turel, J. Košmrlj, Click-Triazole N2 coordination to transition-metal ions is assisted by a pendant pyridine substituent, Inorg. Chem. 49 (2010) 4820–4829, https://doi.org/10.1021/ic902354e.
[27] K.J. Kilpin, E.L. Gavey, C.J. McAdam, C.B. Anderson, S.J. Lind, C.C. Keep, K. C. Gordon, J.D. Crowley, Palladium(II) complexes of readily functionalized bidentate 2-Pyridyl-1,2,3-triazole "Click" ligands: a synthetic, structural, spectroscopic, and computational study, Inorg. Chem. 50 (2011) 6334–6346, https://doi.org/10.1021/ic200789b.
[28] P.M. Guha, H. Phan, J.S. Kinyon, W.S. Brotherton, K. Sreenath, J.T. Simmons, Z. Wang, R.J. Clark, N.S. Dalal, M. Shatruk, L. Zhu, Structurally diverse copper(II) complexes of polyaza ligands containing 1,2,3-triazoles: site selectivity and magnetic properties, Inorg. Chem. 51 (2012) 3465–3477, https://doi.org/10.1021/ic2021319.
[29] W. Yan, X. Ye, N.G. Akhmedov, J.L. Petersen, X. Shi, 1,2,3-triazole: unique ligand in promoting iron-catalyzed propargyl alcohol dehydration, Org. Lett. 14 (2012) 2358–2361, https://doi.org/10.1021/ol300778e.
[30] O. Martínez-Ferraté, C. Werlé, G. Franciò, W. Leitner, Aminotriazole Mn(I) complexes as effective catalysts for transfer hydrogenation of ketones, ChemCatChem 10 (2018) 4514–4518, https://doi.org/10.1002/cctc.201800953.
[31] C. Richardson, P.J. Steel, Benzotriazole as a structural component in chelating and bridging heterocyclic ligands; ruthenium, palladium, copper and silver complexes, Dalton Trans. (2003) 992–1000, https://doi.org/10.1039/b206990c.
[32] S. García-Abellán, D. Barrena-Espés, J. Munarriz, V. Passarelli, M. Iglesias, Cobalt-catalysed nucleophilic fluorination in organic carbonates, Dalton Trans. 52 (2023) 4585–4594, https://doi.org/10.1039/D3DT00731F.
[33] D. Schweinfurth, R. Pattacini, S. Strobel, B. Sarkar, New 1,2,3-triazole ligands through click reactions and their palladium and platinum complexes, Dalton Trans. (2009) 9291, https://doi.org/10.1039/b910660j.
[34] Y. Yang, W. Hu, X. Ye, D. Wang, X. Shi, Preparation of triazole gold(III) complex as an effective catalyst for the synthesis of *E* -α-haloenones, Adv. Synth. Catal. 358 (2016) 2583–2588, https://doi.org/10.1002/adsc.201600243.
[35] S. García-Abellán, A. Pérez-García, D. Barrena-Espés, M.A. Casado, J. Munarriz, V. Passarelli, M. Iglesias, Hemilability modulation via phosphane-triazole ligand design: impact on catalytic formic acid dehydrogenation, Inorg. Chem. (2025), https://doi.org/10.1021/acs.inorgchem.5c03962.
[36] R. van Putten, E.A. Uslamin, M. Garbe, C. Liu, A. Gonzalez-de-Castro, M. Lutz, K. Junge, E.J.M. Hensen, M. Beller, L. Lefort, E.A. Pidko, Non-pincer-type manganese complexes as efficient catalysts for the hydrogenation of esters, Angew. Chem. Int. Ed. 56 (2017) 7531–7534, https://doi.org/10.1002/anie.201701365.
[37] C. Liu, R. Van Putten, P.O. Kulyaev, G.A. Filonenko, E.A. Pidko, Computational insights into the catalytic role of the base promoters in ester hydrogenation with homogeneous non-pincer-based Mn-P,N catalyst, J. Catal. 363 (2018) 136–143, https://doi.org/10.1016/j.jcat.2018.04.018.
[38] V. Vigneswaran, S.N. MacMillan, D.C. Lacy, β-amino phosphine Mn catalysts for 1,4-transfer hydrogenation of chalcones and allylic alcohol isomerization, Organometallics 38 (2019) 4387–4391, https://doi.org/10.1021/acs.organomet.9b00692.

[39] Z. Császár, R. Kovács, M. Fonyó, J. Simon, A. Bényei, G. Lendvay, J. Bakos, G. Farkas, Testing the role of the backbone length using bidentate and tridentate ligands in manganese-catalyzed asymmetric hydrogenation, Mol. Catal. 529 (2022) 112531, https://doi.org/10.1016/j.mcat.2022.112531.
[40] K. Azouzi, A. Bruneau-Voisine, L. Vendier, J.-B. Sortais, S. Bastin, Asymmetric transfer hydrogenation of ketones promoted by manganese(I) pre-catalysts supported by bidentate aminophosphines, Catal. Commun. 142 (2020) 106040, https://doi.org/10.1016/j.catcom.2020.106040.
[41] D. Wei, A. Bruneau-Voisine, T. Chauvin, V. Dorcet, T. Roisnel, D.A. Valyaev, N. Lugan, J. Sortais, Hydrogenation of carbonyl derivatives catalysed by manganese complexes bearing bidentate pyridinyl-phosphine ligands, Adv. Synth. Catal. 360 (2018) 676–681, https://doi.org/10.1002/adsc.201701115.
[42] S.M.W. Rahaman, D.K. Pandey, O. Rivada-Wheelaghan, A. Dubey, R.R. Fayzullin, J.R. Khusnutdinova, Hydrogenation of alkenes catalyzed by a non-pincer Mn complex, ChemCatChem 12 (2020) 5912–5918, https://doi.org/10.1002/cctc.202001158.
[43] C. Rabijasz, S. Weber, B. Stöger, K. Kirchner, Synthesis and application of PN-supported Mn(I) carbonyl alkyl complexes, Organometallics 44 (2025) 1006–1011, https://doi.org/10.1021/acs.organomet.5c00095.
[44] A.M. King, H.A. Sparkes, R.L. Wingad, D.F. Wass, Manganese diphosphine and phosphinoamine complexes are effective catalysts for the production of biofuel alcohols *via* the guerbet reaction, Organometallics 39 (2020) 3873–3878, https://doi.org/10.1021/acs.organomet.0c00588.
[45] M. Roca Jungfer, J.L. Schwarz, F. Rominger, T. Oeser, R. Paciello, A.S.K. Hashmi, T. Schaub, H_2 pressure dependence in the homogeneously catalyzed guerbet reaction of ethanol to butanol using Mn(I) and Ru(II), ChemCatChem 16 (2024) e202301588, https://doi.org/10.1002/cctc.202301588.
[46] A. Luque-Gómez, D. Barrena-Espés, P. García-Orduña, A. Pérez-García, M. A. Casado, J. Munarriz, M. Iglesias, A homobimetallic frustrated lewis pair cobalt catalyst for the methanolysis of hydrosilanes, Angew. Chem. Int. Ed. 64 (2025) e202513522, https://doi.org/10.1002/anie.202513522.
[47] D.V. Gutsulyak, L.G. Kuzmina, J.A.K. Howard, S.F. Vyboishchikov, G.I. Nikonov, $Cp(Pr^{i}{}_{2}MeP)FeH_{2}SiR_{3}$: Nonclassical iron silyl dihydrid, J. Am. Chem. Soc. 130 (2008) 3732–3733, https://doi.org/10.1021/ja800983n.
[48] T.Y. Lee, L. Dang, Z. Zhou, C.H. Yeung, Z. Lin, C.P. Lau, Nonclassical ruthenium silyl dihydride complexes TpRu(PPh3)(η3 -HSiR3 H) [Tp = Hydridotris(pyrazolyl) borate]: catalytic hydrolytic oxidation of organosilanes to silanols with TpRu (PPh3)(η3 -HSiR3 H), Eur. J. Inorg. Chem. 2010 (2010) 5675–5684, https://doi.org/10.1002/ejic.201000951.
[49] M.E. Fasulo, E. Calimano, J.M. Buchanan, T.D. Tilley, Multiple Si–H bond activations by $^{t}Bu_{2}PCH_{2}CH_{2}P^{t}Bu_{2}$ and $^{t}Bu_{2}PCH_{2}P^{t}Bu_{2}$ Di(phosphine) complexes of rhodium and iridium, Organometallics 32 (2013) 1016–1028, https://doi.org/10.1021/om300943e.
[50] R.N. Perutz, S. Sabo-Etienne, The σ-CAM mechanism: σ complexes as the basis of σ-bond metathesis at late-transition-metal centers, Angew. Chem. Int. Ed. 46 (2007) 2578–2592, https://doi.org/10.1002/anie.200603224.
[51] S. Kozuch, S. Shaik, How to conceptualize catalytic cycles? The energetic span model, Acc. Chem. Res. 44 (2011) 101–110, https://doi.org/10.1021/ar1000956.
[52] SAINT+: Area-Detector Integration Software, version 6.01; Bruker AXS: Madison, WI, 2001.
[53] G.M. Sheldrick, SADABS program, University of Göttingen, Göttingen, Germany, 1999.
[54] G.M. Sheldrick, SHELXS 97, Program for the Solution of Crystal Structure, University of Gottingen, Gottingen, 1997.
[55] G.M. Sheldrick, Crystal structure refinement with *SHELXL*, Acta Cryst 71 (2015) 3–8, https://doi.org/10.1107/S2053229614024218.
[56] L.J. Farrugia, WinGX and ORTEP for Windows: an update, J. Appl. Cryst. 45 (2012) 849–854, https://doi.org/10.1107/S0021889812029111.
[57] Frisch, M. J., Trucks, G. W., Schlegel, H. B., Scuseria, G. E., Robb, M. A., Cheeseman, J. R., Scalmani, G., Barone, V., Petersson, G. A., Nakatsuji, H., Li, X., Caricato, M., Marenich, A. V., Bloino, J., Janesko, B. G., Gomperts, R., Mennucci, B., Hratchian, H. P., Ortiz, J. V., Izmaylov, A. F., Sonnenberg, J. L., Williams-Young, D., Ding, F., Lipparini, F., Egidi, F., Goings, J., Peng, B., Petrone, A., Henderson, T., Ranasinghe, D., Zakrzewski, V. G., Gao, J., Rega, N., Zheng, G., Liang, W., Hada, M., Ehara, M., Toyota, K., Fukuda, R., Hasegawa, J., Ishida, M., Nakajima, T., Honda, Y., Kitao, O., Vreven, T., Throssell, K., Montgomery, J. A., Jr., Peralta, J. E., Ogliaro, F., Bearpark, M. J., Heyd, J. J., Brothers, E. N., Kudin, K. N., Staroverov, V. N., Keith, T. A., Kobayashi, R., Normand, J., Raghavachari, K., Rendell, A. P., Burant, J. C., Iyengar, S. S., Tomasi, J., Cossi, M., Millam, J. M., Klene, M., Adamo, C., Cammi, R., Ochterski, J. W., Martin, R. L., Morokuma, K., Farkas, O., Foresman, J. B., Fox, D. J., Gaussian 16, Revision C.01, (2016).
[58] Y. Zhao, D.G. Truhlar, A new local density functional for main-group thermochemistry, transition metal bonding, thermochemical kinetics, and noncovalent interactions, The J. Chem. Phys. 125 (2006) 194101, https://doi.org/10.1063/1.2370993.
[59] A. Luque-Gómez, D. Barrena-Espés, P. García-Orduña, A. Pérez-García, M. A. Casado, J. Munarriz, M. Iglesias, A homobimetallic frustrated lewis pair cobalt catalyst for the methanolysis of hydrosilanes, Angew. Chem. Int. Ed. (2025) e202513522, https://doi.org/10.1002/anie.202513522.
[60] S.E. Neale, D.A. Pantazis, S.A. Macgregor, Accurate computed spin-state energetics for Co(iii) complexes: implications for modelling homogeneous catalysis, Dalton Trans. 49 (2020) 6478–6487, https://doi.org/10.1039/D0DT00993H.
[61] K.P. Jensen, J. Cirera, Accurate computed enthalpies of spin crossover in iron and cobalt complexes, J. Phys. Chem. A 113 (2009) 10033–10039, https://doi.org/10.1021/jp900654j.
[62] H.P. Bhattacharyya, M. Sarma, Role of active centers in predicting the catalyst turnover: a theoretical study, Chem Eur J 30 (2024) e202403631, https://doi.org/10.1002/chem.202403631.
[63] H.-Q. Mo, C. Hou, Mechanistic and machine learning insights into borrowing hydrogen reactions catalyzed by transition metal complexes with N-heterocyclic ligands, Org. Chem. Front. (2025), https://doi.org/10.1039/D5QO01139F.
[64] F. Weigend, R. Ahlrichs, Balanced basis sets of split valence, triple zeta valence and quadruple zeta valence quality for H to Rn: Design and assessment of accuracy, Phys. Chem. Chem. Phys. 7 (2005) 3297, https://doi.org/10.1039/b508541a.
[65] A.V. Marenich, C.J. Cramer, D.G. Truhlar, Universal solvation model based on solute electron density and on a continuum model of the solvent defined by the bulk dielectric constant and atomic surface tensions, J. Phys. Chem. B 113 (2009) 6378–6396, https://doi.org/10.1021/jp810292n.
[66] R. Tanaka, M. Yamashita, L.W. Chung, K. Morokuma, K. Nozaki, Mechanistic studies on the reversible hydrogenation of carbon dioxide catalyzed by an Ir-PNP complex, Organometallics 30 (2011) 6742–6750, https://doi.org/10.1021/om2010172.
[67] Legault, C. Y., CYLview, (2009).